Dual-Axial Blood Pump Mechanical Circulatory Support for Fontan Patients

A Thesis

Submitted to the Faculty

of

Drexel University

by

Shravani N Birewar

in partial fulfillment of the

requirements for the degree

of

Master of Science

in Biomedical Engineering

May 2016

Acknowledgments

I would like to take this opportunity to thank a number of people for their contribution and support towards this thesis.

First, I would like to thank my advisor, Dr. Amy Throckmorton, for her guidance throughout this process. She has made significant contributions towards my thesis, from generating the device models and meshes to providing me with ample resources to successfully complete my thesis. Dr. Throckmorton has been an amazing mentor, challenged me to work my hardest, and has had a tremendous amount of confidence in me throughout the project.

Additionally, I would like to thank Dr. Sriram Balasubramanian and Dr. Wan Shih for taking the time to serve on my committee and for providing their valuable insights on my thesis.

I appreciate the assistance and support of those both currently and previously at the BioCirc Research Laboratory. Sarah Haynes and Nohra Murad contributed much of their time towards running the large number of simulations needed for data analysis. Dr. Steven Chopski and Carson Fox have been greatly encouraging and helpful by sharing their knowledge and experiences.

Last but not least, I want to thank my pillars of strength: my family and friends. I am grateful to my friends and my brother, who have motivated and encouraged me to be persistent in my goals. Most of all, my parents are my inspiration, and I am truly thankful for their love, care, and for being there for me at every step.

Table of Contents

List of Tables

List of Figures

Abstract

Dual-Axial Blood Pump Mechanical Circulatory
Support for Fontan Patients

Shravani Birewar

The current treatment paradigm for patients with dysfunctional or failing single ventricle physiology involves pharmacologic therapy, surgical reconstruction of the Fontan physiology, and heart transplantation. The limited number of donor hearts and complication of a Fontan surgical takedown require alternative treatment strategies for these patients. Existing mechanical circulatory support systems are inadequate for these patients since these devices were designed for the systemic circulation in patients with a biventricular circulation, not a Fontan physiology. Therefore, researchers have been developing new blood pumps for single ventricle patients. As a new therapeutic approach, this thesis considers a newly combined configuration of dual-axial flow blood pumps located in the pulmonary arteries to mechanically support the Fontan physiology. The initial design geometries were constructed using computer-aided design software. Pump design equations and empirical data were utilized to create the differing design configurations based on pump placement, diameter, protective cage filaments, stagger angle, blade number, and operational states. The pump performance of these configurations was assessed using robust ANSYS CFX turbomachinery software. Over 150 simulations were performed over a range of blood flow rates and rotational speeds. Pressure rise, energy augmentation, and

blood damage indices were determined for the pump geometries considered. All simulations showed pressure and energy augmentations within and above the needed range for improved cavopulmonary conditions. Additionally, all simulations examined for blood trauma showed mean blood damage indices below 1%. Overall, the current research was successful and demonstrated significant proof-of-concept support in the development of a dual-support approach for patients having dysfunctional or failing Fontan physiology.

1. Motivation and Significance

1.1 Motivation and Significance

Globally, two million children are born with a congenital heart defect every year [1]. Cardiovascular defects are attributed to 6-10% of all infant deaths. Without surgical or therapeutic intervention, a patient with significant cardiac malformations, such as those with severe defects or only a single functioning ventricle, would rapidly decompensate to congestive heart failure (CHF), resulting in death within two weeks after birth [2]. Patients with single ventricle physiology require long-term intensive management, monitoring, and therapy to slow the inevitable decline to CHF. The clinical treatment and management of patients having congenital heart defects costs approximately $1.4 billion per year, while the incidence of single ventricle physiology occurs 1 in 2000 births per year [3, 4].

1.1.1 Normal Physiology

In contrast to a single ventricle physiology and for distinguishing purposes, a healthy heart is divided into four chambers: the left and right ventricles and the left and right atria (**Figure 1**). The left and right atria receive blood from the pulmonary and systemic circulations, respectively. The pulmonary veins lead to the left atrium, and the superior and inferior vena cavae (SVC and IVC) lead to the right atrium. The blood then passes through valves to enter into the

ventricles. The ventricles act as pumps to generate the necessary pressure for blood to travel into the systemic and pulmonary circuits. The right ventricle pushes blood into the left and right pulmonary (LPA and RPA) arteries that lead to the lungs, and the left ventricle pushes blood into the aorta, which branches to supply blood to the rest of the body.

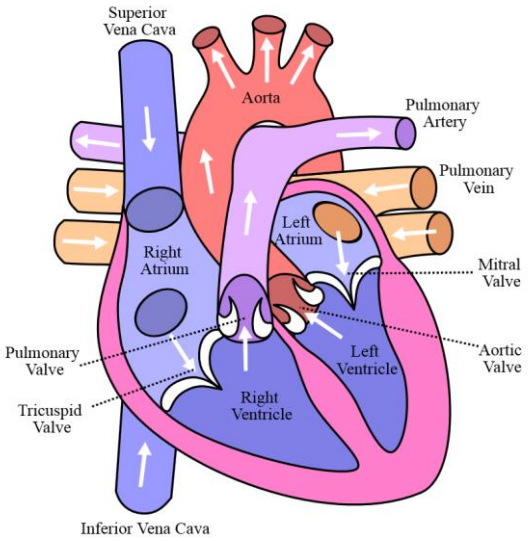

Figure 1: Diagram of the normal physiology of a human heart and blood flow [5].

1.1.2 Single Ventricle and the Fontan Procedure

Contrary to a normal physiology, a single ventricle or Fontan physiology consists of only one functional ventricle to both drive and draw blood through the systemic and pulmonary circulations. In order to achieve the Fontan physiology, patients must undergo 3 or more open-heart, staged surgeries as discussed in the following paragraphs.

The open-heart procedures are called the Norwood procedure, the Glenn (or Hemi-Fontan), and the Fontan completion. The Norwood procedure occurs at two weeks of age, where an artery-to-pulmonary-artery shunt is created to allow blood flow to the lungs. The second procedure (the Glenn) involves making a connection between the superior vena cava and the pulmonary arteries and removing the Norwood shunt. This procedure is done at age 6 weeks. The final procedure, performed at the age of 3-5 years, is the Fontan procedure, which connects the inferior vena cava to the pulmonary arteries. This culminates in the final Fontan physiology that has a new vessel configuration that is called the total cavopulmonary connection (TCPC), where the inferior and superior vena cavae connect directly to the pulmonary arteries (as seen in **Figure 2**). This results in deoxygenated blood flowing directly to the pulmonary circuit rather than entering the right atrium to be pumped through the heart [2].

The TCPC physiology has cardiovascular benefits. It reduces the burden on the functioning ventricle by reducing the volume overload on the ventricle, and it normalizes arterial saturation. Moreover, it uses the energy from the capillaries to push the blood through the pulmonary system [6]. Additional surgical improvements have resulted in better blood flow and minimized scarring [1]. Overall, the Fontan physiology improves the life expectancy of the patients; however, long-term consequences of this 'human-made' physiology exist, and there are extremely few medical devices or therapeutic options beyond the early staged surgical procedures.

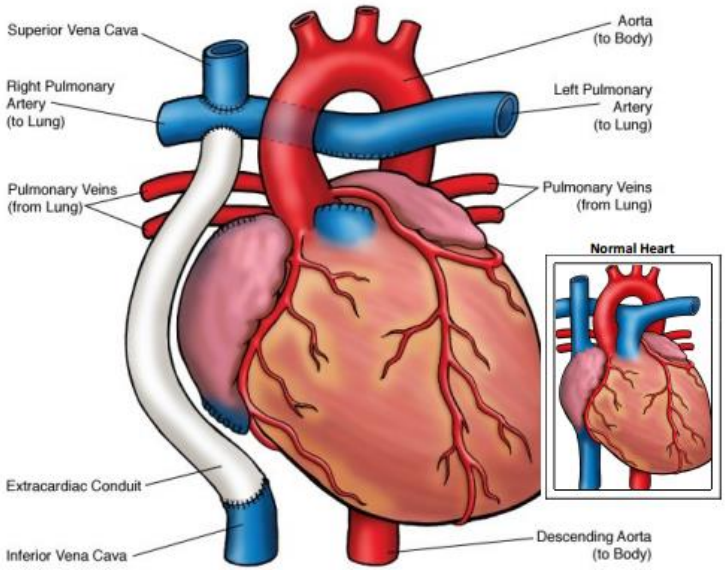

Figure 2: Diagram of the extracardiac TCPC configuration with a side comparison of normal heart vasculature [7].

1.1.3 Concerns of the TCPC

Although the improvements from this procedure are realized in the short-term, the patients still encounter physical and functional limitations associated with normal daily activities. Fontan patients have abnormal cardiovascular hemodynamics, increased systemic venous pressure, supraventricular arrhythmias, and reduced exercise capacity [2]. Fontan patients also have displayed the inability to increase stroke volume during exercise due to a decrease in end-diastolic volume [8]. Additionally, 15% of Fontan patients have protein-losing enteropathy. These symptoms result in a general decline to premature CHF, as seen in more than 40% of patients with a TCPC [9].

A number of surgical interventions exist to assist with complications of the Fontan physiology, but these approaches only slow the progression of CHF. Interventions include reinclusion of previously excluded hepatic veins, baffle fenestration, atrioventricular valve repairs or replacements, pacemaker insertions, revisions to a lateral tunnel or an extra-cardiac Fontan, and a number of simple repair procedures. However, in the case of ventricular dysfunction or a failing Fontan circulation, cardiac transplantation is currently the only therapeutic option for the patients. Though there are a number of surgical interventions, cardiac transplantation is often a necessity for Fontan patients, which is challenging [10]. Apart from the long wait associated with waiting for a donor organ, Fontan patients are faced with a greater early mortality rate in comparison to non-Fontan patients with congenital heart disease or with cardiomyopathy [9, 10]. The reconstruction of the systemic and pulmonary veins and the pulmonary arteries also make the transplant surgery a significant challenge [10]. In fact, the statistics demonstrate a 44% operative mortality rate for cardiac transplantations [2]. With these challenges, it is necessary to have new therapeutic solutions using innovative devices. Researchers and clinicians have hypothesized that an increase in pressure of 1 - 5mmHg in the Fontan circulation will produce improved physiological conditions for single ventricle patients [1]. To address this unmet therapeutic need, the BioCirc Laboratory at Drexel University is developing a novel intravascular blood pump to provide mechanical circulatory support of the cavopulmonary circulation in Fontan patients. Our long-term

objective is to provide a viable bridge-to-transplant therapeutic option for these Fontan patients.

1.2 Existing Mechanical Assist Devices

In addition to the development effort in our research laboratory, there are currently mechanical circulatory support systems that are being used for Fontan patients and several researchers are designing new devices to mechanically support the dysfunctional or failing single ventricle physiology. The following sections detail the existing technology being used for Fontan patients and the new technology that is under development.

1.2.1 Extracorporeal Membrane Oxygenation

Extracorporeal membrane oxygenation (ECMO) is often utilized to support patients with congenital or other forms of heart disease. Morbidity and mortality with ECMO support is very high, ranging from 33% to 60%. Although cases of ECMO support for Fontan patients exist, not many studies provide a strong understanding of its capabilities [11]. Rood et al. [11] analyzed ECMO utilization for cardiac failure after Fontan operation. Only 35% of patients survived hospital discharge. Causes of mortality included surgical bleeding, renal failure, and neurologic complications. On the other hand, 47% survival was reported for pediatric cardiac patients who received ECMO support. This clinical data

demonstrates the ongoing challenges associated with ECMO utilization for Fontan patients.

1.2.2 Ventricular Assist Devices

In contrast to ECMO, alternative medical devices that are used to support CHF patients are ventricular assist devices (VADs). VADs can support the left or right ventricles of the heart [12]. There are currently various types of VADs on the market. VADs can have pulsatile or continuous flow, which can have either a centrifugal or axial design. Additionally, VADs can be defined by the location of the pumps: intracorporeal, paracorporeal, and extracorporeal [13].

A frequently used VAD, named Berlin Heart EXCOR, is often employed as a bridge-to-transplant device for pediatric and adult patients. A study was done with 48 children to evaluate EXCOR performance. The results showed that EXCOR was successful for 88% of the patients as a bridge-to-transplant or bridge-to-recovery therapeutic. The median duration for support was 28 days [13]. Additionally, a study conducted by Weinstein et al. [14] with twenty-six patients demonstrated that EXCOR can be used over a long duration for patients with single ventricle physiology as a bridge to cardiac transplantation. However, the overall success rate of utilizing EXCOR for single ventricle patients was 42%. Additionally, studies have shown adverse effects like infection, stroke, and bleeding post-implantation of the device [13]. Other challenges of the Berlin Heart EXCOR include mobility. Patients implanted with this device have limited mobility. A small and portable driving system exists for the biventricular

configuration. However the battery life of the driver is limited to five hours. Additionally, this device is limited to adult patients. Pediatric patients are confined to the Ikus drive system, a 93kg drive unit [12].

One of the major limitations with the current VADs on the market is that these devices are designed for supporting the systemic circulation and biventricular support rather than single ventricle support and a physiology with a TCPC. Thus, these devices produce significantly higher pressures than desired for the Fontan physiology [15]. For example, Jarvik 2000, by Jarvik Heart Inc., is an axial flow left VAD. Although, the design is able to support right ventricles by reducing the rotational speeds (6000-10000 RPM) to provide the needed pulmonary pressures, the design has not been changed to be able to support the right ventricle [12].

1.2.3 Cavopulmonary Support Devices

No cavopulmonary assist devices (CPAD) currently exist for clinical use. However, several research labs are in the process of developing these devices or testing existing devices to serve as cavopulmonary support.

Lacour-Gayet et al. [16] developed an artificial right ventricle design. This new model was developed with a conduit connecting the SVC and IVC. The conduit then forms a pathway (where an axial pump is placed) to the LPA and RPA. Although this design showed improvement in circulatory function within *in vitro* studies, its major drawback is that it requires complete reconstruction of the Fontan physiology.

Medvitz et al. [17] developed an extracardiac implant for full circulatory support. This design involved a Tesla design pump that utilized closely spaced parallel plates rather than impeller blades. Although this design showed positive hydrodynamic performance, it requires an invasive surgical procedure and is not designed for a Fontan physiology. The device is also significantly obstructive and could result in patient death if the pump fails or stops due to thrombus formation or mechanical failure. Similarly, Wang et al. [18] discussed an extracardiac concept, which combines their previously designed double lumen cannula (DLC) and a commercially available blood pump (CentriMag) as a cavopulmonary assist device. Based on this design, the DLC withdraws blood from the SVC and IVC and pumps the blood through a bridge graft into the RPA.

Less invasive solutions have also been proposed by various researchers. Wang et al. [19] developed model with a DLC placed in the TCPC with two collapsible membrane umbrellas and a pump in the SVC. While the pump supports circulation, the umbrellas increase efficiency of the pump by preventing backflows. A temporary cavopulmonary support device by Giridharan et al. [20] involves an expandable viscous impeller pump with an expandable nitinol cage, and is located in the TCPC junction. The pump can be inserted percutaneously. Researchers showed a 23% increase in cardiac output in mock circulatory system experiments with this design. Axial blood pumps are also being researched and have shown promising results as cavopulmonary support devices. Wang et al. [21] developed a microaxial flow pump for placement in the IVC that has shown some success in computational and in vitro studies. Also,

Rodefeld et al. [22] implanted the Hemopump, an axial flow pump, in both vena cavae in yearling sheep that had undergone surgery to develop a total cavopulmonary diversion. This study demonstrated the application of nonpulsatile axial flow pumps to provide cavopulmonary support, thus showing the prospective benefits of CPAD devices.

1.2.4 Limitations of Devices Under Development

Even though devices are under development to support Fontan patients, there are many limitations of these pump designs. **Table 1** highlights those limitations. Many of these devices discussed require invasive surgeries or have the risk of causing obstruction in the blood vessels. Additionally, blood stagnation, high shear stresses and blood damage can also result from some designs. Thus, a mechanical circulatory support is needed that can address these limitations in **Table 1**.

Table 1: Cavopulmonary support devices currently under development and their limitations

Device	Limitations
Artificial Right Ventricle with Extracardiac Conduit	• Requires reconstruction of Fontan
Extracardiac Device with Tesla pump	• Requires invasive surgery • Not designed for Fontan physiology • Severely obstructive if device fails
DLC and CentriMag	• Does not provide bidirectional lung perfusion • Requires invasive surgery
DLC, Pump, and Collapsible Umbrellas	• Blood stagnation at umbrellas can lead to thrombosis
Expandable Viscous Impeller Pump	• Failure can result in obstruction of TCPC • Patient must have cross-like vessel configuration
Microaxial Flow Pump	• Retrograde flow into SVC
Hemopump	• Can result in high blood damage and backflow into SVC

1.3 New Solution: Dual-Axial Device Combination

To address the limitations of existing devices and the clinical need for an implantable mechanical circulatory support in the cavopulmonary circulation of Fontan patients and to advance the current state-of-the-art in mechanical circulatory assistance, a unique design is under development in the BioCirc Research Laboratory at Drexel University.

The BioCirc Research Laboratory has performed a significant amount of research to evaluate axial continuous flow pump performance in the TCPC and address the issues with Fontan physiology discussed. An axial flow pump design

has been shown to be successful through hydraulic and hemolysis testing at the BioCirc Lab. The desired hydraulic energy was generated, shear stresses were below 425 Pa, and the normalized index of hemolysis (N.I.H.) levels met design objectives [23].

The pump placement in the IVC has also been extensively evaluated. This placement has shown success in terms of pressure and energy augmentation [24]. However, due to the increased pressure generation and a greater IVC flow rate and pressure than SVC flow rate and pressure (due to the 60%/40% IVC/SVC split), retrograde flow into the SVC can result with higher rotational speeds. Additionally, in a normal physiology, the IVC blood carries liver factors that are crucial for lung function and development. It is necessary that the IVC blood flows into both the left and right pulmonary arteries to the lungs [25]. When the pump is placed in the IVC, the anatomical geometry of the TCPC shunts more IVC blood toward the RPA. However, research has shown that an even distribution of flow can be accomplished with reduced blood vorticity of IVC blood when entering the TCPC. This was achieved by placement of the pump below the hepatic flow connection in the IVC [24].

A dual-pump support has also been evaluated by placement of axial flow pumps in the SVC and the IVC. This prospective design showed positive results in pressure augmentation and hydraulic energy generation in computational analysis using the anatomical TCPC model. It also demonstrated low scalar stresses and residence times. However, blood damage results were higher than

the 2% criteria. Overall, this study showed that dual-pump designs can be utilized and can show positive results but require optimization [9].

The addition of a cage supporting the axial pump has also been studied. A cage is required for pump support and vessel wall protection. Studies showed that varying twists of the cage filaments can boost energy transfer generated by the impeller and reduce blood damage when compared to straight filaments [26, 27].

Many studies done in the past have analyzed pump performance in an anatomical TCPC model. This was achieved by converting 2-D MRI images to 3-D CAD models. It has been experimentally shown that the axial flow blood pump design is a viable therapeutic option in the anatomical TCPC [25].

To ameliorate the likelihood of retrograde blood flow into the SVC toward the brain, we are considering a new design. This novel design consists of a combination of a catheter, stent, and two axial pumps for dual mechanical support of the right and left pulmonary arteries. The catheter is T-shaped and allows for implantation of the two axial pumps. The stent in the design connects the SVC and IVC in the TCPC to direct blood flow for collection at the pump inlets. The axial pumps are placed into the left and right pulmonary arteries. The rotational action of the axial pumps propels the blood gathered from the stent into the pulmonary arteries. The overall goal of this configuration is to provide the amount of pressure needed for Fontan patients to have near-normal circulation as a bridge-to-transplant support system. The performance of this configuration will be simulated using computational fluid dynamic simulations.

This thesis is a proof-of-concept for this unique design developed in the BioCirc Research Laboratory. The design, seen below, incorporates successful aspects of the pump devices previously developed in the lab and seeks to overcome some of their design limitations.

The model geometry was developed using SolidWorks 2014 and can be seen below in **Figure 3**. As discussed, BioCirc Laboratory has examined pump performance in patient-specific TCPC models. However, for the purpose of the initial evaluation of this novel design, the mechanical assist device was modeled within an idealized TCPC. The SVC and IVC (20mm diameters) and pulmonary arteries (25mm diameters) were modeled with ideal cylindrical structures. The vena cavae and pulmonary arteries intersect perpendicularly in this model.

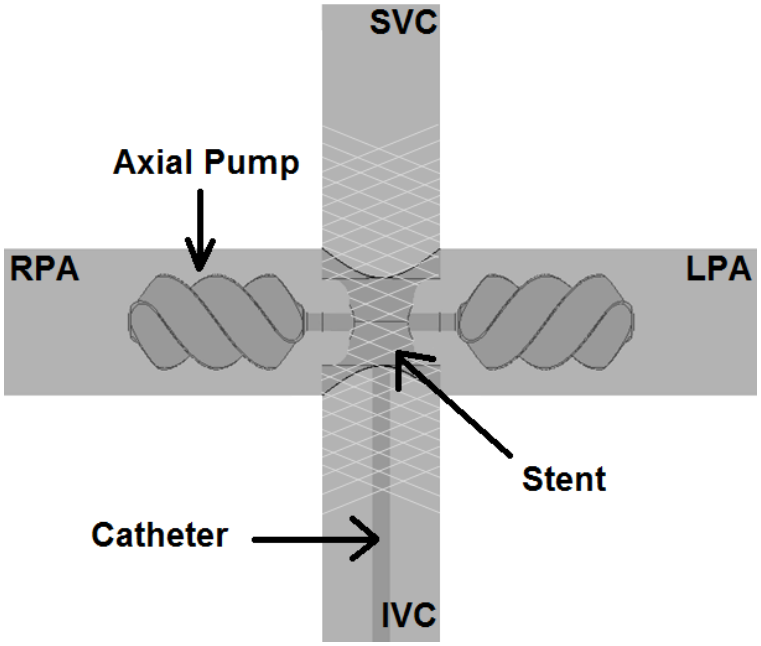

Figure 3: Conceptual design of the double axial blood pump and stent configuration. LPA: left pulmonary artery; RPA: right pulmonary artery; SVC: superior vena cava; IVC: inferior vena cava

The lumen stent in the design connects the SVC and IVC. This stent narrows in the center to allow for blood flow between the LPA and RPA, and also allows for blood collection from SVC and IVC. The stent was created using the lofting tool in SolidWorks, with the central inner diameter as approximately 10.86 mm. Additionally, the stent consists of two circular openings on the lateral and medial sides through which the blood exits to reach the axial pumps.

As discussed previously, continuous axial flow pumps designed in the BioCirc Laboratory have been shown to be effective in generating pressure and hydraulic energy, while minimizing blood damage and shear stresses. Thus, these axial pumps were utilized for the purpose of this design. The pumps have helically wrapped blades around the central hub. The angled blades extend with a width of 16.15 mm and the pumps have lengths of 30.5 mm. The two axial pumps are located in the LPA and RPA. This is in contrast to the previous studies conducted with a singular pump positioned in the IVC or dual pumps located in the IVC and SVC. The positioning in the pulmonary arteries and dual pump configuration serves to overcome the few design limitations discussed with the previous designs. This pump placement eliminates the risk of SVC backflow with increasing rotational speed. Instead, the pumps would generate suction pressure in the vena cavae, further encouraging blood collection in the stent. Additionally, this placement would eliminate vorticity in the IVC, thus allowing equal IVC and SVC blood flow into both arteries. Both pumps would then propel equal amounts of blood flow to each lung. Therefore, both lungs receive equal levels of liver factors.

The final aspect of the design is the catheter that will be utilized to percutaneously insert the pumps. The catheter has a 3.05 mm outer diameter. It is located in the SVC and branches in the stent to exit through its two openings and attaches to the pumps.

In summary, this configuration would collect blood from the SVC and IVC and generate hydraulic energy to drive the blood through the pulmonary arteries. The axial pumps can create a suction effect to pull the blood from the stent and generate hydraulic energy to increase blood flow and reduce fluid congestion in the pulmonary arteries due to hypotension. This, in turn, would result in an increase in cardiac output and systemic blood flow. Overall, this design serves the functions of the right atrium and ventricle and seeks to resolve the long-term problems associated with the Fontan.

2. Design

2.1 Problem Statement

Thousands of Fontan patients have a dysfunctional single ventricle physiology. Although the Fontan procedure is the preferred surgical intervention for congenital heart defects with single ventricles, various issues are associated with the Fontan circulation. Due to the TCPC physiology, no subpulmonary power source or right ventricle exist to drive blood into the pulmonary arteries. Additionally, as the blood from the SVC and IVC meet at the TCPC, mixing results in turbulent flow and energy losses as the blood enters the pulmonary arteries. Symptoms of the Fontan physiology, such as abnormal cardiovascular hemodynamics, increased systemic venous pressure, supraventricular arrhythmias, and protein-losing enteropathy have resulted in premature heart failure in many Fontan patients [2]. Lack of therapeutic solutions, complications associated with cardiac transplantation, and high treatment costs despite the low number of patients have led to a critical need for mechanical pump solutions for Fontan patients.

2.2 Thesis Project Objectives

This project focuses on the proof-of-concept of a novel design approach. The overall goal of this thesis is to develop a new mechanical circulatory support configuration at the total cavopulmonary connection (TCPC) that is able to

improve physiological conditions for a Fontan patient suffering from dysfunctional single ventricle physiology. Detailed below are the four specific objectives of this project:

1. Design a new dual-support configuration having a venous return collection stent in the TCPC of a Fontan physiology with mechanical circulatory assistance in the pulmonary arteries.

The goal is to design a system that serves the purpose of the right atrium and ventricle of the heart. Thus, the design must appropriately allow for the collection of blood from the SVC and IVC at the TCPC and be directed to mechanical pumps. The pumps must be able to propel the blood through the pulmonary arteries.

2. Develop and optimize the pump geometries, and determine inflow conditions, blood parameters, and design factors.

In this objective, the configuration is designed by defining a number of parameters. The geometries and dimensions of the axial pumps and stent are determined, while considering the size constraints due to the dimensions of the TCPC. Additionally, the inflow conditions and blood parameters are selected to closely represent physiological conditions in the TCPC. A number of design factors are chosen to analyze their effect on pump performance.

3. Determine the shear stresses, pressure generation, energy gain, and blood damage indices in consideration of biophysical factors.

A number of factors must be evaluated to understand the efficiency of the design. Firstly, pressure and hydraulic energy generations are needed to augment flow through the pulmonary arteries. Additionally, shear stresses must be evaluated for prevention of blood trauma. Blood damage index must also be calculated to ensure minimal hemolysis due to the design. The analysis of these values will help to determine whether the design factors chosen in **Objective 2** play a significant role in the pump performance.

4. Determine optimal ranges of design factors to analyze their contribution to pump performance and confirm the feasibility of the design.

By determining the ranges of the design factors that meet the necessary requirements in **Objective 3**, a conclusion can be made on whether the design can meet the necessary expectations needed for Fontan patients. As mentioned, the overall goal of this design is to improve the quality of living for Fontan patients by improving the physiological conditions in their circulatory system. This specific objective seeks to ensure that the axial pumps accomplish this goal through the implementation of necessary enhancements based on the analysis from **Objective 3**.

2.3 Design Requirements - General

There are a number of constraints and requirements that must be met to develop a design that meets the patient needs and address the current limitations in the existing mechanical assist devices. First of all, the device must be made of biocompatible material and must be non-thrombogenic. Additionally, device implantation must be a minimally invasive process to diminish surgical and post-surgical complications and allow for a shorter recovery period. The device should also have an operative lifespan sufficiently larger than the current wait time periods of Fontan patients for heart transplants. Also, the device should be cost-effective.

Regarding the device structure, the lumen stent should allow blood to be collected from the IVC and SVC but should not restrict flow between the LPA and RPA. The stent must have two outlets, and must be able to direct blood in both directions (into the LPA and RPA). The openings of the stent that lead to the pumps should not be so small to result in a significant pressure buildup in the stent. It is also important to ensure that the pump blades do not contact the blood vessel while the patient is still or in motion. Blades contacting the vessel while the impeller is in motion could damage and rupture the blood vessel. Lastly, the pump must be large enough to tolerate and propel the blood, with consideration of its mechanical properties (viscosity, density, flow rate, etc.).

2.4 Engineering Standards to Inform Design

Table 2 includes a list of standards reviewed for their level of applicability to the current project. Three ASTM standards were assessed to determine whether they can be employed for this thesis or for future studies.

ASTM F1841-97 standardizes hemolysis testing for continuous flow blood pumps. Hemolysis testing can help determine the level of blood trauma caused by the continuous flow blood pump design. However, it does not involve any aspects of computational modeling, thus this standard would be a necessity in the future when the design is experimentally tested *in vitro*. ASTM F1830-97 standardizes the selection of blood for the standardized hemolysis testing method. Thus, this would also be a required standard in the future when the design is tested *in vitro*. Lastly, ASTM F2514-08 standardizes finite element modeling for a metallic stent. The standard is not entirely applicable to the current project as it is meant for another device. However, it includes software requirements, standards in developing the mesh, and additional steps that must be taken to validate and verify the analysis. These aspects of the standard can be referred to for the models that will be developed for the design.

Table 2: List of ASTM standards that can be applied to the evaluation of the device.

Standard	Title
ASTM: F1841 − 97	Standard Practice for Assessment of Hemolysis in Continuous Flow Blood Pumps
ASTM: F1830 − 97	Standard Practice for Selection of Blood for *in vitro* Evaluation of Blood Pumps
ASTM: F2514 − 08	Finite Element Analysis (FEA) of Metallic Vascular Stents Subjected to Uniform Radial Loading

2.5 Performance Criteria

It has been demonstrated through prior research that a pressure generation of 1 - 5mmHg within the cardiovascular circulation is required to bring the circulation to near-normal physiological conditions [1]. Hence, the energy gain is important to compute as it helps determine the impact of the pumps on the energy of the system. By calculating change in hydraulic energy, it can be determined whether the axial pumps are effective in generating any energy gain in the pulmonary arteries [28]. Sufficient pressure and energy generation will allow the system to serve the purpose of an artificial right ventricle by pushing the blood through the pulmonary arteries. Increased pressure reduces fluid congestion in the pulmonary arteries while increasing cardiac output, thus reducing many of the symptoms observed in Fontan patients.

In consideration of blood trauma in a rotating machine, such as a blood pump, we seek to ensure that shear stress levels remain below 425Pa and exposure time below 620ms [29]. It is also desired that blood damage indices

remain below 2% [30].For these reasons, shear stress, pressure generation, and blood damage indices are determined.

2.6 Design Factors

For the simulations, the following design factors were chosen to evaluate: IVC/SVC flow rate, pump rotational speed, rotational speed difference between pumps, twist angle of impeller blades, cage design, and LPA/RPA outlet pressures.

Table 3 lists the ranges and variations selected for the design factors. Venous return flow rates were evaluated at 1-4 L/min. This is representative of flow rates in resting Fontan patients [31]. For rotational speed, 2000, 3000, and 4000 RPM were selected because previous research has shown pressure rises meeting design criteria with rotational speeds of 2000 to 6000 RPM for one pump [32]. A lower range was chosen for the current analysis as this design has two axial pumps and more shear stresses and blood damage can result. Additionally, further understanding was developed of the effects of varying rotational speeds on pressure generations by evaluating the pumps with unequal rotational speeds. Previous studies at BioCirc have evaluated twist angle of the impeller blades from 60-600° at higher rotational speeds and showed high pressure rises in cases above 100° [33]. This study evaluated a middle range (200-500°) at lower rotational speeds to evaluate whether the new configuration can demonstrate pressure rises within the same ranges. **Figure 4** to **Figure 7** show the models created to represent pumps with varying blade twist angles. As discussed earlier,

studies have shown that cage filaments assist energy transfer by the impeller rotation. Thus, two cage filament patterns will be assessed to understand the contribution of the design in generating hydraulic energy. The models generated for straight and twisted filaments can be seen in **Figure 8** and **Figure 9**, respectively. LPA and RPA were chosen to have equal pressures and were evaluated in the 9mmHg - 24mmHg range. Mean pulmonary arterial pressure is approximately 15mmHg, while pressure during diastole can reach 8mmHg [34, 35]. Fontan physiology results in an elevated pulmonary vascular resistance, for which reason the higher range of pressures are also being evaluated [36].

Table 3: List of design factors evaluated for proof-of-concept of device

Design Factors	Ranges Evaluated
Inlet Flow Rates (IVC/SVC)	1-4 L/min
Pump Rotational Speeds	2000, 3000, 4000 RPM
Unequal Pump Rotational Speeds	+1000, +500, -500, -1000 RPM (Left-Right)
Twist Angle of Pump Blades	200°, 300°, 400°, 500°
Cage Design	Straight, twisted filaments
Outlet Pressures (LPA/RPA)	9mmHg - 24mmHg

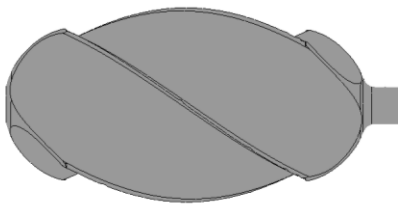

Figure 4: 200° impeller

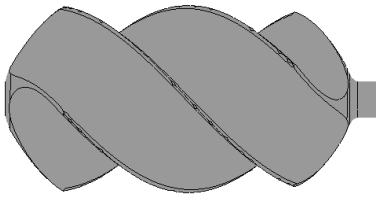

Figure 5: 300° impeller

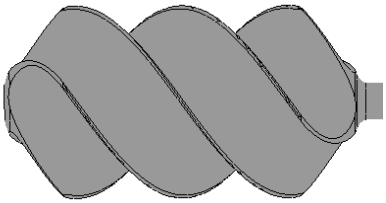

Figure 6: 400° impeller (original)

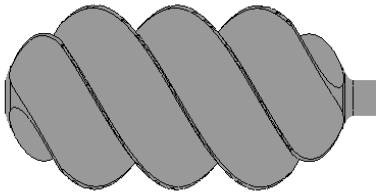

Figure 7: 500° impeller

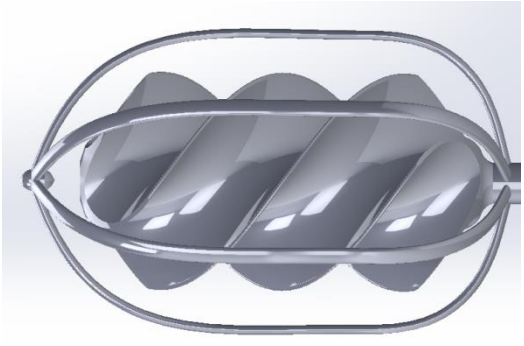

Figure 8: Straight cage design

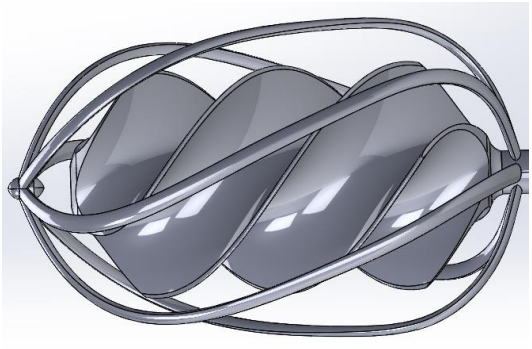

Figure 9: Twisted cage design

3. Computational Methods

3.1 Background

As in this thesis project, computational methods have long been used for simulations of the Fontan physiology to analyze hemodynamics in the system and in the development of rotary blood pumps for placement and implementation in the cardiovascular system. Computational fluid dynamics (CFD) analyses have also been utilized to surgically optimize the TCPC through examination of flow dynamics and energy losses. Various configurations of the TCPC exist, and researchers continue to optimize the physiology through examination of factors, such as shear stresses and flow stagnation, to improve long-term health of patients [37]. This study will also utilize CFD analysis methods to simulate and analyze the coupling of the mechanical pump design with the TCPC. Thus, design factors can be computationally evaluated to optimize pump performance.

3.3 Computational Fluid Dynamics

ANSYS CFX 15.0 software (ANSYS, Inc., Canonsburg, PA, USA) was employed to execute computational fluid dynamics analysis within the TCPC with the insertion of this pump design. The CFX-Mesh program was used to generate a mesh of tetrahedral elements for each of the three-dimensional model components developed in SolidWorks [24].

The generated mesh components were imported and assembled into the ANSYS-CFX solver. The CFX-Solver uses a hybrid finite-element/finite-volume approach to solve the Reynolds-averaged Navier-Stokes equations for each simulation. The program solves for turbulent flow conditions in the model.

ANSYS-CFX runs the simulation, as seen in **Figure 10**, until the solution reaches the pre-set convergence value of 1 x 10^{-3} [38]. This value provides a tolerance for the acceptable accuracy of the approximation [39]. Once the simulation has converged, post-processing tools from CFX-Post are used to visualize and analyze the results of the CFD simulations.

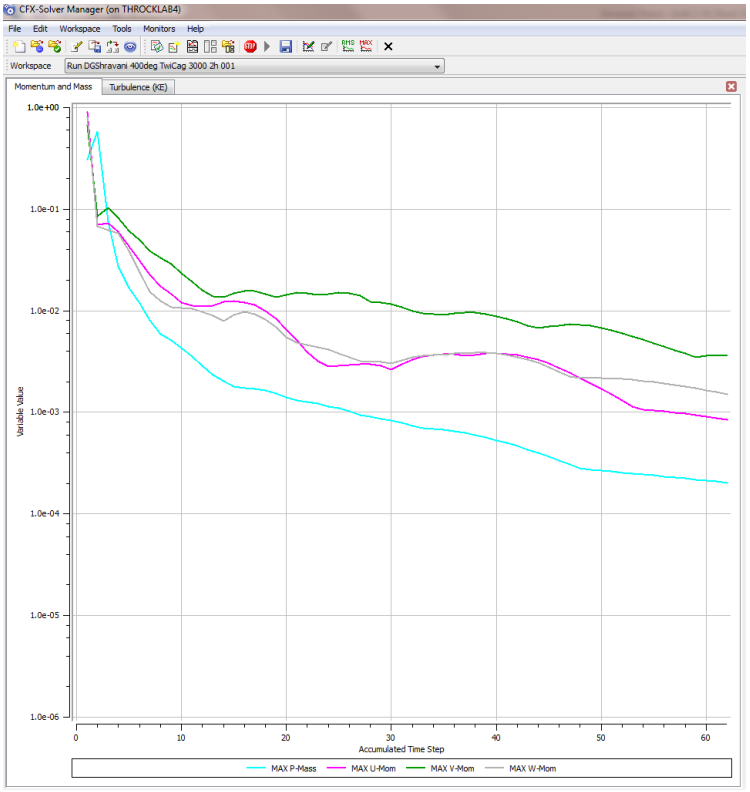

Figure 10: CFX-Solver for one of the simulations as convergence value approaches 1 x 10^{-3}

3.3.1 Navier-Stokes Equations

The fluid solver of the ANSYS CFX solves the Navier-Stokes equations. The Navier-Stokes equations are derived from the conservation of momentum equations. The conservation of mass equation, as seen in **Equation 1**, is developed based on the concept that mass flow into a controlled volume must equal mass flow out of the volume [38].

$$\frac{\partial \rho}{\partial t} + \frac{\partial}{\partial x_i}(\rho U_i) = 0$$

Equation 1: Conservation of Mass

In the equation above, U_i is the velocity vector of flow, t is time, and ρ is the fluid density. The conservation equation of momentum, ρU_i, can then be developed:

$$\frac{\partial}{\partial t}(\rho U_i) + \frac{\partial}{\partial x_j}\left(\rho U_i U_j\right) = -\frac{\partial P}{\partial x_i} - \frac{\partial \tau_{ij}}{\partial x_j} + \rho f_i$$

Equation 2: Conservation of Momentum

In **Equation 2**, x_i and x_j are the special variables, P is the pressure, τ_{ij} is the viscous stress tensor, and f_i is the body force vector. The gravity component of the equation is not considered in **Equation 2** for the purpose of this analysis as the force of gravity is negligible in comparison to the centripetal force generated by the rotary axial pump. The stress tensor can be further defined as

below for a Newtonian fluid (displays a linear relationship between shear stress and shear strain rate) [38, 39].

$$\tau_{ij} = -\mu_b \delta_{ij} \frac{\partial U_k}{\partial x_k} - \mu_v \left(\frac{\partial U_i}{\partial x_j} - \frac{\partial U_j}{\partial x_i} \right)$$

Equation 3: Viscous stress tensor equation

In **Equation 3**, μ_v is the dynamic viscosity, μ_b represents the bulk viscosity ($2/3 * \mu_v$), and δ_{ij} is the Kronecker delta [38].

3.3.2 Reynolds Averaging Navier Stokes (RANS) Method

In turbulent flow conditions, variable quantities tend to fluctuate continuously. For this reason, the Reynolds-averaging procedure is used. This method defines the scalar values as the sum of the mean and fluctuating components.

With the application of the Reynolds-Averaging form and the assumption that flow is of an incompressible fluid displaying constant density, **Equations 1-3** become the following:

$$\frac{\partial \bar{U}_i}{\partial x_i} = 0$$

Equation 4: Averaged conservation of mass

$$\frac{\partial}{\partial t}(\rho \bar{U}_i) + \frac{\partial}{\partial x_j}\left(\rho \bar{U}_i \bar{U}_j\right) = -\frac{\partial \bar{P}}{\partial x_i} - \frac{\partial}{\partial x_j}(\tau_{ij} + \rho u_i u_j)$$

Equation 5: Averaged conservation of momentum

$$\overline{\tau_{ij}} = -\mu_v \left(\frac{\partial \overline{U}_i}{\partial x_j} - \frac{\partial \overline{U}_j}{\partial x_i} \right)$$

Equation 6: Averaged viscous stress tensor for an incompressible fluid

ANSYS-CFX utilizes this Reynolds-averaged Navier-Stokes method to approximate the flow conditions in the pump. The challenge with this method is the emergence of higher-order correlations in the flow equations, which result in a “closure problem”. In order to determine these correlations or unknown stress tensor components, a closure model is required [38, 39].

3.3.2 Turbulence Modeling

The Reynolds number (Re) was calculated using the equation below. Based on the calculation, Re is on the order of 10^4, thus showing that turbulent flow dominates in the system [40]. This supports the use of turbulence modeling for the computational analysis.

$$Re = \frac{\omega r L \rho}{\mu} = 23{,}200$$

Equation 7: Reynolds number equation

A κ-ε turbulence model was used "to close" the simulation-based equations. A study comparing different turbulence models showed that the κ-ε model had the best correlation to the experimental data, within a 10-20% range [40]. This model utilizes two transport equations to further analyze the turbulence conditions and allows for equation closure. This model solves the two equations

for κ and ε. The κ represents the turbulent kinetic energy and the ε is the dissipation rate [38, 41]. The dissipation rate can be further elaborated as the quantity of κ per mass and time that is converted to internal fluid energy. Turbulent kinetic energy can be related to the turbulent velocity scale (V_t) with the following relationship: $\kappa = V_t^2$. The dissipation rate of κ can be determined with the following equation:

$$\varepsilon = \frac{\kappa^{3/2}}{l_t}$$

Equation 8: Equation relating turbulent kinetic energy and dissipation rate

In the above equation, l_t represents the turbulent length scale. Both κ and ε can then be utilized to determine the turbulent viscosity (μ_t). Thus, turbulence modeling allows the estimation of turbulent viscosity and turbulence kinetic energy to approximate the flow equations in the free shear regions [38].

3.3.3 Boundary and Flow Conditions for the Simulations

Simulations were performed under steady flow conditions with the assumption that the vessel walls are rigid. No slip boundary conditions were applied to the solid boundaries, which include the catheter wall, TCPC vessel walls, stent, and blades of the two pumps. The pump boundaries were defined in the rotating reference frame. Additionally, the boundary between the IVC vessel wall and catheter wall, and boundaries surrounding the pump rotors were defined as fluid-fluid interfaces. These boundaries were created for developing the mesh;

however no actual wall will exist in the real design. The fluid-fluid boundary condition allows for the unrestrictive flow of fluid between the two areas. The mass inflow rate was split as 60%/40% for the IVC/SVC. For the simulations, fluid viscosity of 0.0035 kg/m*s and density of 1050 kg/m^3 were selected to represent blood properties. Fluid viscosity of 0.0035 kg/m*s (3.5 cP) corresponds to a hematocrit of approximately 33%. This is characteristic of blood properties of pediatric patients with congestive heart disease [38].

3.3.4 Blood Damage Modeling

With blood contacting the rotating surfaces in blood pumps, there is a risk of hemolysis and thrombosis. For this reason, a blood damage analysis using the CFD models was performed. As mentioned, the goal is to have the stress values below 425Pa for 600 milliseconds, and a blood damage index of less than 2% in development of the double axial blood pump device. To analyze for blood damage, a technique was used to calculate for the six components of stress tensor and scalar stress (σ). The scalar stress values were calculated according to **Equation 9** to estimate the amount of stress endured by the blood.

$$\sigma = \left(\frac{1}{6}\sum\left(\sigma_{ii} - \sigma_{jj}\right)^2 + \sum \sigma_{ij}^2\right)^{1/2}$$

Equation 9: Shear stress

The above equation includes the *i* and *j* components of the stress tensor. Blood damage index can be calculated based on the power law relationship between scalar stress and particle exposure time as shown in **Equation 10**.

$$\frac{dHb}{Hb} = C \times \sigma^{\alpha} \times T^{\beta}$$

Equation 10: Change in hemoglobin content

In **Equation 10**, dHb represents the change in hemoglobin content from blood damage, Hb denotes hemoglobin content, σ is the scalar stress (calculated in **Equation 9**), and T is the fluid exposure time to the scalar stress. C, α, and β all represent proportionality constants determined through the regression of experimental data. To calculate for scalar stress and particle exposure time, fluid streamlines were analyzed by simulating the release of 350 particles within the system. Both scalar stress and exposure time were summed for the streamlines. Based on **Equation 10**, the following power law equation can be used to determine the possibility of blood cell damage as it passes through the axial blood pumps.

$$D = \sum_{inlet}^{outlet} (1.8 \times 10^{-6}) \times \sigma^{1.991} \times \Delta t^{0.765}$$

Equation 11: Blood damage index

D represents the blood damage index, t is the exposure time, and σ is the scalar stress. Inlet indicates the entrance of the fluid flow (SVC and IVC), and outlet represents the exit (LPA and RPA). As derived from **Equation 10**, D

represents the percent difference in hemoglobin levels, which occurred due to blood damage, divided by the initial hemoglobin quantity [28]. To complete this calculation, an analysis code was utilized with the MATLAB program (Matlab, The Mathworks Inc., Natick, MA, USA). Based on the design criteria, D below 0.02 (2%) is sought for this design. The constant and exponential values in **Equation 11** were determined with experimental data regression in a Couette viscometer. The study had fluid stress of 40 to 700Pa with exposure times of 0.0034 to 0.6 seconds. These values are representative of stress and exposure time levels found in blood pumps [42, 43]. **Table 4** represents the conditions tested for blood damage indices, including rotational speed, flow rate, degree twist of blades, outlet pressures, and cage design.

3.3.5 Energy Augmentation Estimations

A control volume approach was used to determine the energy generated in the pulmonary arteries. With the below equations, the amount of energy that would be gained or lost with both axial pumps can be estimated:

$$E_{loss} = -\sum (P_{static} + 0.5\rho u_k u_k) u_i n_i A_i$$

$$= \sum \left(P_{total\_in}\right) Q_{inlet} - \sum \left(P_{total\_out}\right) Q_{outlet}$$

Equation 12:Energy loss

$$P_{total} = \overline{P_{static}} + 0.5\rho \overline{u_i u_i}$$

Equation 13: Total pressure

$$Q_i = u_i A_i$$

Equation 14: Flow rate

In the above equations, E_{loss} is the rate of energy consumption in the pulmonary arteries and P_{total} is the total pressure, which includes the static (P_{static}) and kinetic components. Q represents the flow rates at the inlets (SVC and IVC) and outlets (LPA and RPA). The inlet pressures were determined at the point before the pumps and the outlet pressures were determined at the point after the pumps. This represented the total pressure and allowed for estimation of total energy change in the pump regions. Also, u_i and u_k denote the velocity components, while n_i signifies the component of the normal vector of the outer surface and A_i represents the area [28].

4. Computational Results

4.1 Analysis 1: Pump Rotational Speed Variation

Pump performance at varying rotational speeds was modeled with CFD simulations. These conditions were evaluated and utilized for comparisons with condition and design variations during future experiments. For this analysis, the meshed design included a 400° impeller for each axial pump. Additionally, these conditions included a set blood viscosity of 0.0035 kg/m*s and density of 1050 kg/m^3. The inlet flow distribution was chosen to be 60% IVC and 40% SVC and outlet pressures of LPA and RPA was set to 18 mmHg. Three different pump rotational speeds were compared for this experiment: 2000 RPM, 3000 RPM, and 4000 RPM. Simulations were run for each rotational speed with varying flow rates: 1.0 to 4.0 L/min at 0.25 L/min intervals.

Figure 11 and **Figure 12** show the pressure generations for each pump and rotational speed with increasing flow rate. Comparison of left and right pumps shows that performance with identical conditions for each pump result in near-identical pump performance. The graphs also demonstrate an increase in pressure generation with increasing rotational speed, and a decrease in pressure generation with increasing flow rate. Pressure generation ranged from approximately 1.84-8.53mmHg, with the greatest pressure increase at 4000 RPM and 1 LPM and the lowest increase at 2000 RPM and 3 LPM. Energy generation in the pulmonary arteries versus flow rate was illustrated in **Figure 13**. This

demonstrated an increase in energy transfer with greater rotational speed and flow rate. Energy increase ranged from 4.57 mW (1 LPM, 2000 RPM) to 65.2 mW (4 LPM, 4000 RPM).

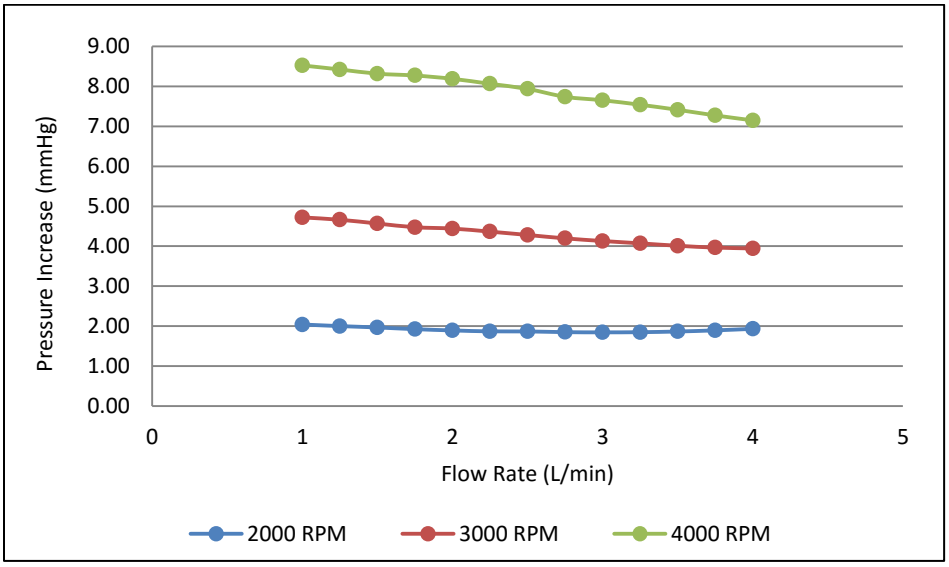

Figure 11: Graphical representation of pressure generation in the left pump region with increasing flow rate for 2000, 3000, 4000 RPM

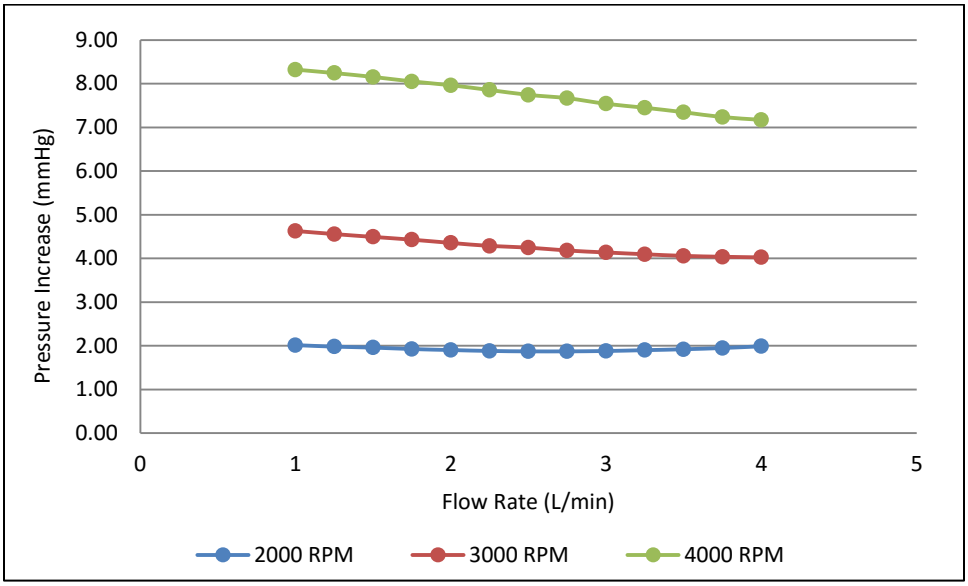

Figure 12: Graphical representation of pressure generation in the right pump region with increasing flow rate for 2000, 3000, 4000 RPM

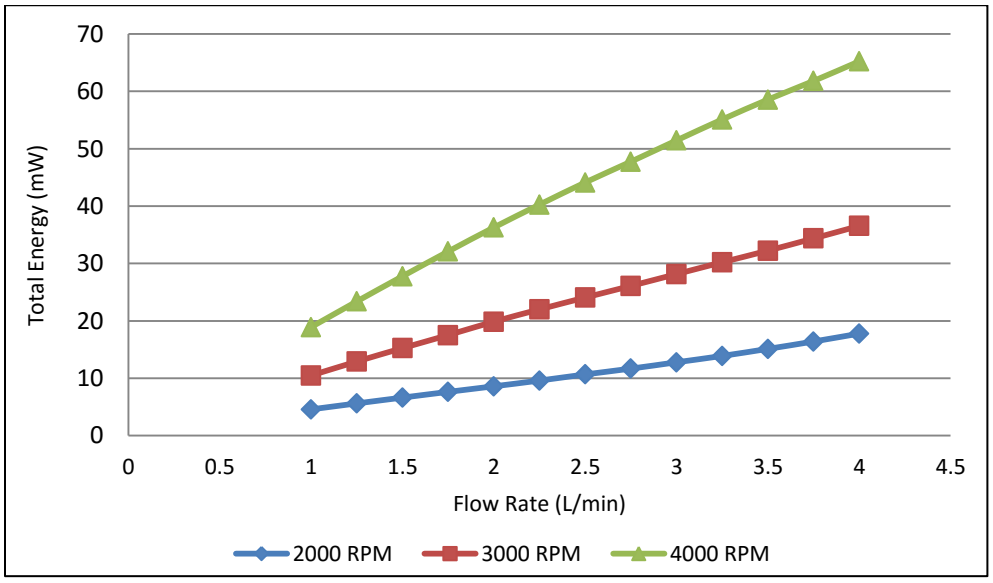

Figure 13: Graphical representation of energy generated in the pulmonary arteries with increasing flow rate for 2000, 3000, 4000 RPM

4.2 Analysis 2: Impeller Blade Degrees Variation

For the second experiment, three additional models were created with different impeller designs. While the original design had pump impellers with 400° twisted blades (**Figure 6**) the new models included 200°, 300°, and 500° impellers (**Figure 4**, **Figure 5**, and **Figure 7**). This analysis compared the pump performance with varying angles of impeller blades. For this analysis, the blood viscosity, blood density, inlet flow distribution, outlet pressures were kept the same as Analysis 1. The flow rate was fixed at 3.0 LPM and each model's performance was simulated at 2000 RPM, 3000 RPM, and 4000 RPM. For this experiment, both pumps were set to equal conditions.

Figure 14 shows the increase in pressure for each rotational speed with increasing twist of the blades for the left pump only. Only the left pump was displayed since Analysis 1 demonstrated that the pumps show similar performances when set to equal conditions. Pressure increase ranges from 1.56 to 8.94mmHg. As seen in **Figure 14**, pressure generation increases with increasing twist and peaks at 300°, after which the pressure generation begins to decrease. For each rotational speed, the lowest pressure generation occurs at 500°. **Figure 15** shows the energy generation in the pulmonary arteries with increasing impeller blade twist for each rotational speed. This showed a range of 11mW (500°, 2000 RPM) - 59mW (300°, 4000 RPM). This demonstrated a similar pattern as the pressure generation graph, with 300° showing the greatest energy generation for each rotational speed and 500° showing the least energy generation for all rotational speeds.

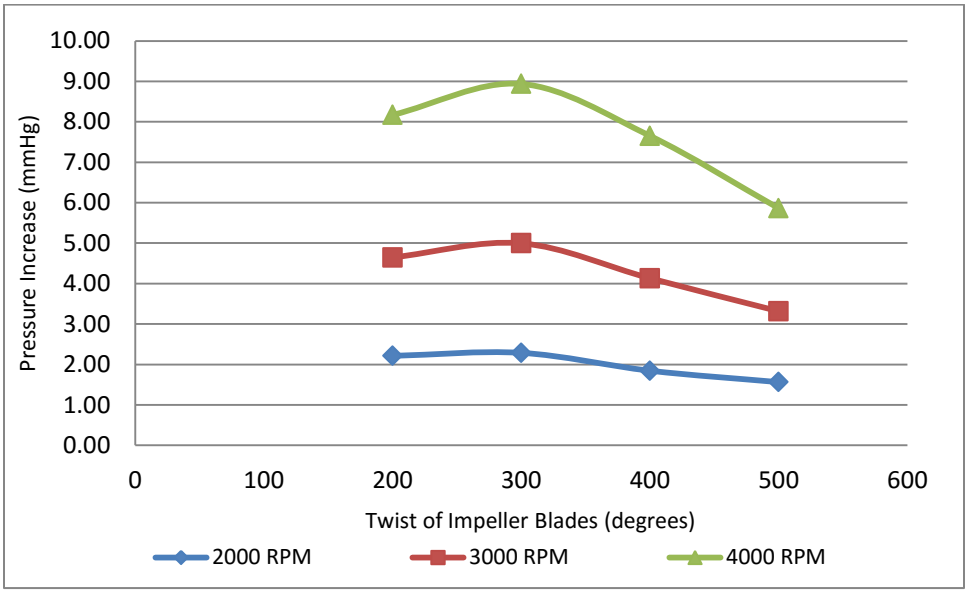

Figure 14: Graphical representation of pressure generation in the left pump region with increasing twist of impeller blade for 2000, 3000, 4000 RPM

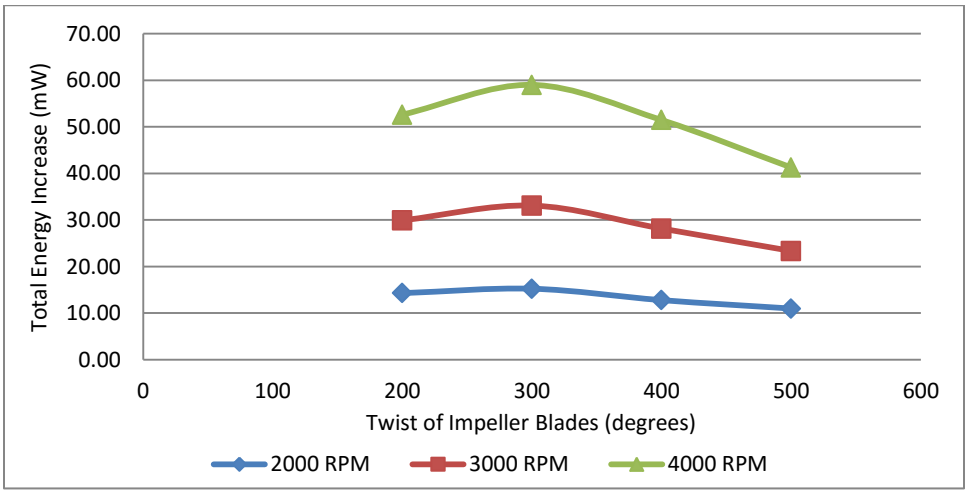

Figure 15: Graphical representation of energy generation in the pulmonary arteries with increasing twist of impeller for 2000, 3000, 4000 RPM

4.3 Analysis 3: Unequal RPMs

For this next experiment, the left and right pumps had unequal RPMs to examine how significant these changes are on pump performance. For this analysis, the left pump was fixed at 3000 RPM and the right pump was varied from 2000 RPM to 4000 RPM in intervals of 500. All other parameters were kept the same as Analysis 1. Data of both pumps at 3000 RPM was leveraged from Analysis 1 for comparison.

In **Figure 16**, it can be seen that increasing rotational speed in the right pump generated slight but negligible pressure increase in the left pump. As expected in the right pump (**Figure 17**), a significant pressure increase was found with higher RPMs. RPMs in 2000, 2500, and 3000 showed pressure generation within the desired 1 - 5mmHg range. **Figure 18** shows an increasing energy gain with increasing right pump RPM. As expected, the effect of rotational speed on energy generation increases with increasing flow rate.

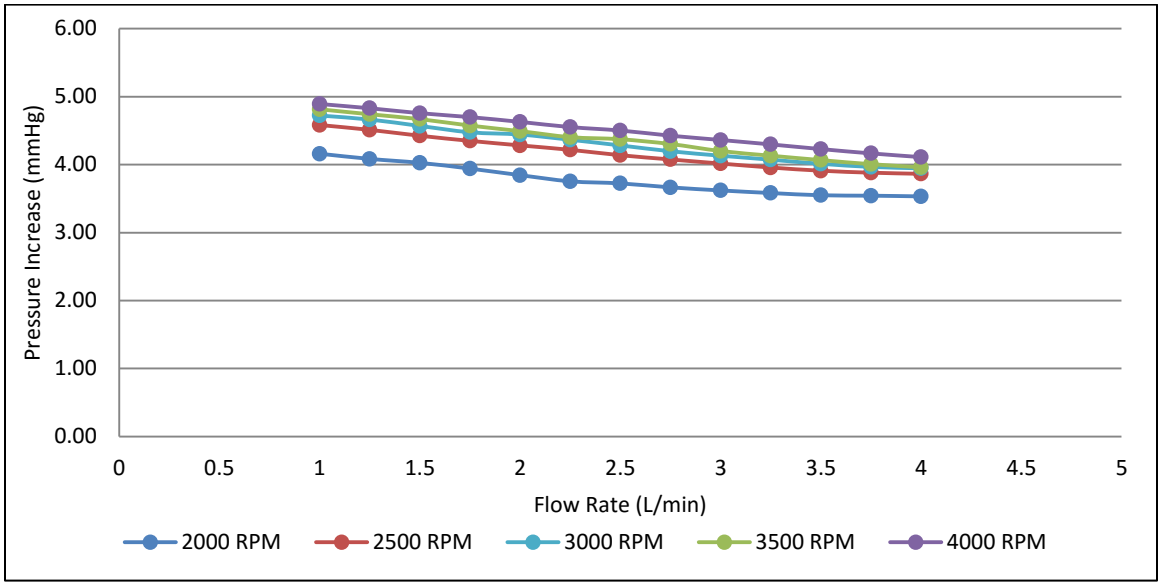

Figure 16: Graphical representation of pressure generation in the left pump region with increasing flow rate for constant left pump RPM (3000 RPM) and varying right pump RPM (2000 – 4000 RPM)

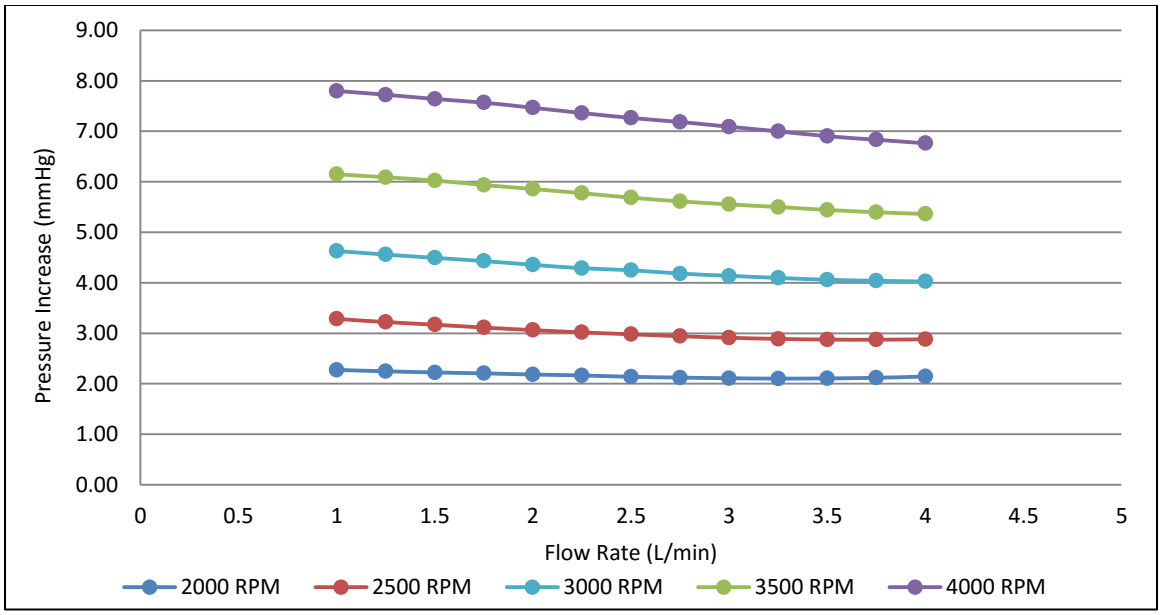

Figure 17: Graphical representation of pressure generation in the right pump region with increasing flow rate for constant left pump RPM (3000 RPM) and varying right pump RPM (2000 – 4000 RPM)

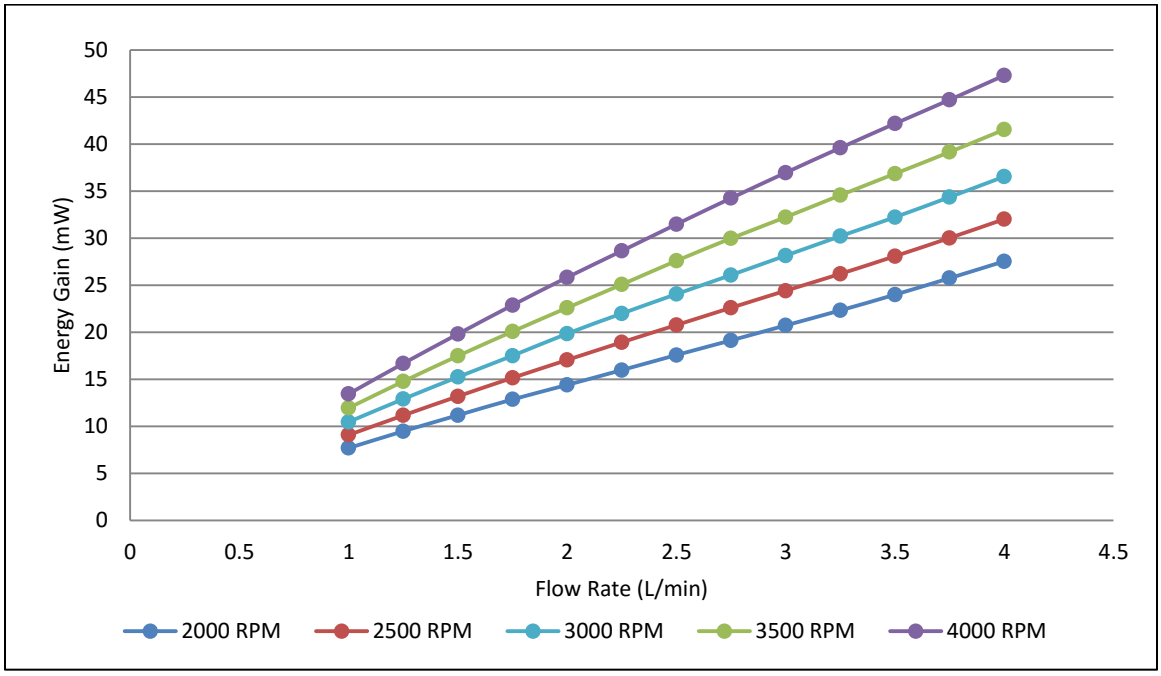

Figure 18: Graphical representation of energy generation in the pulmonary arteries with increasing flow rate for constant left pump RPM (3000 RPM) and varying right pump RPM (2000 – 4000 RPM)

4.4 Analysis 4: Cage Design

Including cages to surround the axial pumps is important for stability as well as vessel protection [26]. This analysis examined the Analysis 1 conditions with pumps at 3000 RPM held within straight and twisted cages. **Figure 8** shows the straight cage design and **Figure 9** shows the twisted cage design. Both cage designs were generated on SolidWorks and new pump models were meshed for the studies. Both cages consisted of 6 filaments surrounding the pump and extending axially. The twisted cage design (**Figure 9**) was such designed that the filaments twist with the blades.

Figure 19 and **Figure 20** show performance comparisons of the two cage design models with data from Analysis 1. For all simulations, left and right pumps were set at 3000 RPM. Both figures show that the insertion of a cage resulted in a significant decrease in pressure and energy generation. The twisted cage design further reduced these values when compared to the straight cage design. Another observation was that the insertion of a cage reduced the level of effect flow rate had on pressure and energy generation.

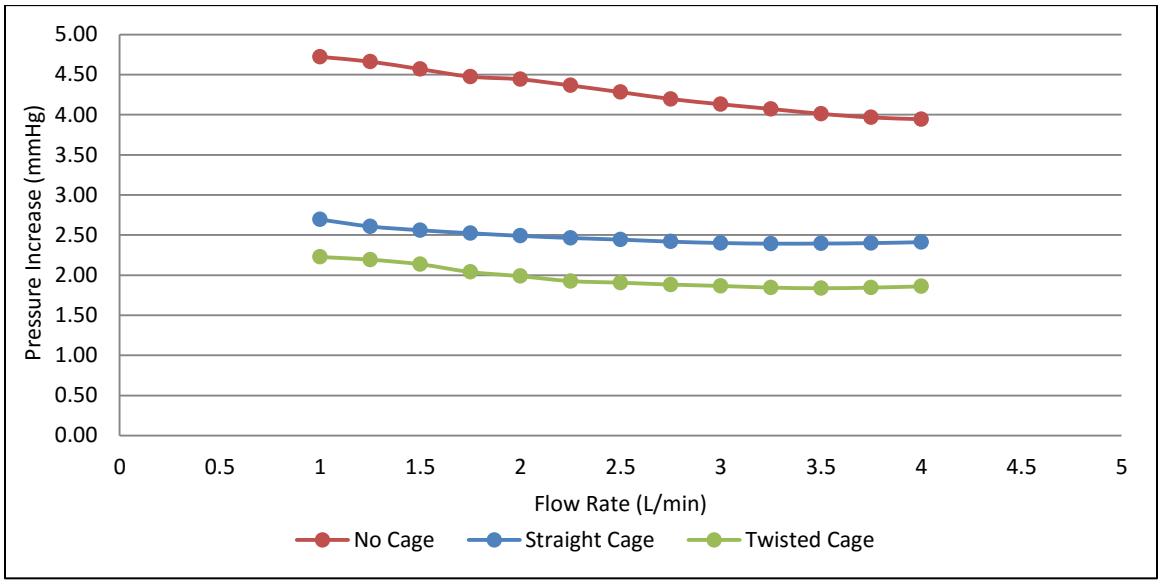

Figure 19: Graphical representation of pressure generation in the left pump region with increasing flow rate for no cage, straight cage, and twisted cage designs

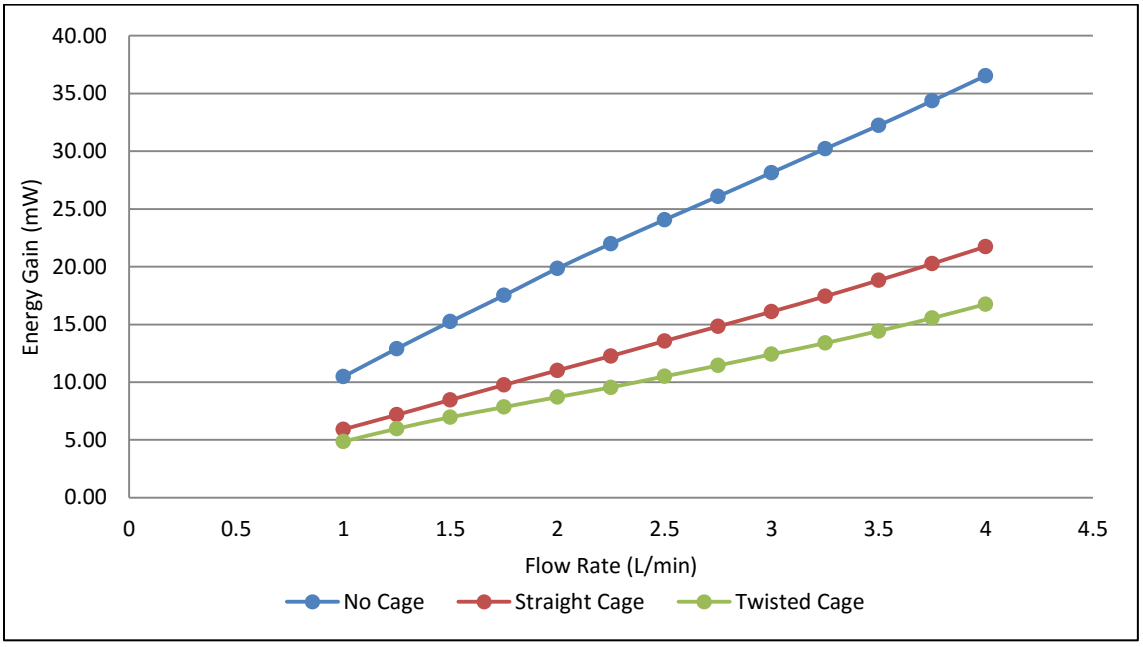

Figure 20: Graphical representation of energy generation in the pulmonary arteries with increasing flow rate for no cage, straight cage, and twisted cage designs

4.5 Analysis 5: LPA and RPA Variation

The final analysis varied LPA and RPA outlet pressures to examine the change in SVC and IVC inlet pressures. Increasing rotational speed of the pumps when the LPA and RPA outlet pressures are low could theoretically decrease inlet pressures in the SVC and IVC. A significant pressure drop can be detrimental as it could cause the vessel to collapse. Since the SVC constituted a smaller percentage of the flow rate, in comparison to IVC, SVC was expected to show lower inlet pressures. Thus, **Figure 21** plots SVC inlet pressure changes with changing pump RPM for LPA and RPA outlet pressures ranging from 9 to 24mmHg. All simulations for this analysis were done with 3 L/min, 400° impeller

pumps, and a straight cage design. The straight cage design was utilized as it was known a cage design would be required to support the pumps. The 18mmHg LPA and RPA outlet pressure results were leveraged from straight cage design results in Analysis 4.

The results from this analysis show slight decreases in inlet pressures with increasing rotational speed. Increasing RPM from 2000 to 4000 RPM resulted in a pressure drop of less than 5mmHg. Additionally, increasing the outlet pressures by 3mmHg also resulted in 3mmHg increases in SVC pressures. The lowest inlet pressure was 16.49 mmHg when the outlet pressures were 9mmHg and the rotational speed was 4000 RPM.

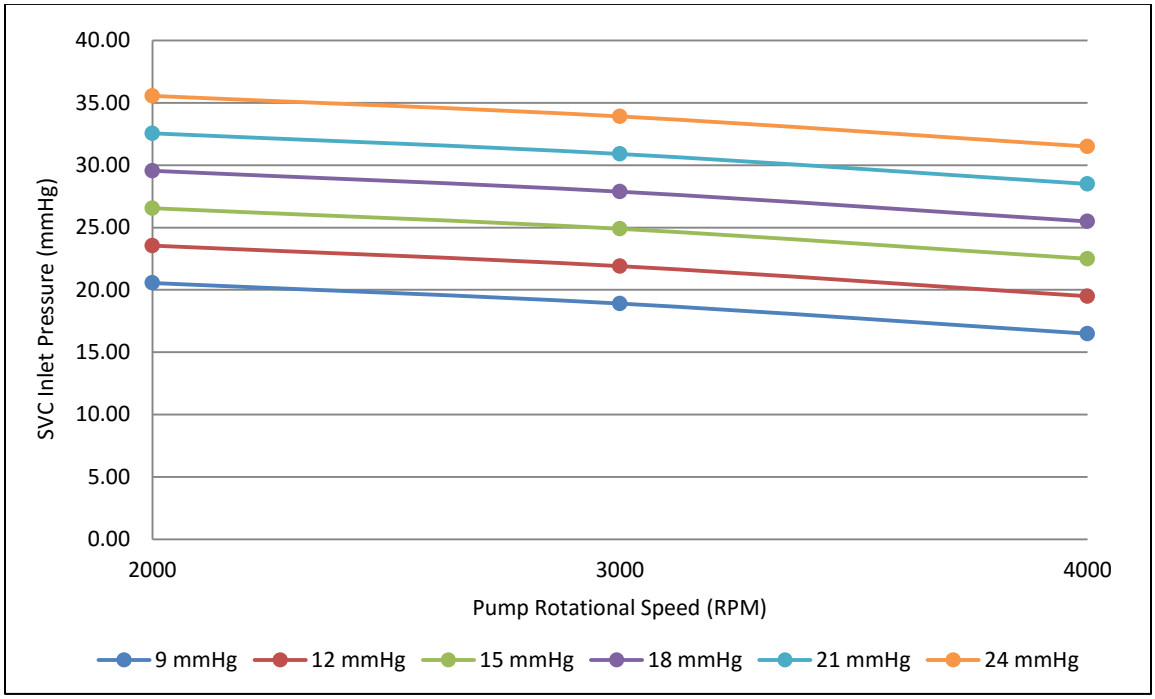

Figure 21: Graphical representation of SVC inlet pressure with increasing rotational speed for varying LPA and RPA outlet pressures

4.6 Blood Damage Analysis

Certain design configurations were analyzed while simulating the release of 350 particles into the system to conduct a blood damage analysis. **Table 4** shows the list of simulations that were analyzed for blood damage indices, total exposure time, and shear stresses. The results include mean and maximum exposure times and damage indices, as well as maximum shear stresses.

Most mean exposure times were approximately 1 second. However, Simulation #1 had the highest mean exposure time at 2.17 seconds. Simulations #12, 13, 14, and 15 had the lowest mean exposure times (all between 0.7-0.8 seconds). Simulations #1, 3, 6, and 10 showed max exposure times greater than 5 seconds, while Simulation #14 showed the lowest maximum exposure time of 1.91 seconds. Examining the damage indices of all simulations showed that the mean damage indices ranged from 0.05% to 0.42%. Simulation #6 had the highest maximum percentage at 0.64%. Maximum shear stresses ranged from 253.3Pa (Simulation #3) to 541.8Pa (Simulation #7).

Table 4: Blood damage analysis with simulations examined and results

Analysis 1											
#	**LPM**	**Impeller (°)**	**Left RPM**	**Right RPM**	**Cage**	**LPA/RPA (mmHg)**	**Time (s): Mean**	**Time (s): Max**	**DI: Mean**	**DI: Max**	**Max Shear Stress**
1	1	400	3000	3000	None	18	2.170	5.167	0.05%	0.05%	346.3
2	2	400	3000	3000	None	18	1.207	3.605	0.08%	0.15%	312.4
3	3	400	2000	2000	None	18	1.171	6.677	0.20%	0.38%	253.3
4	3	400	3000	3000	None	18	0.869	2.260	0.20%	0.37%	269.2
5	3	400	4000	4000	None	18	0.852	3.047	0.22%	0.35%	523.9
6	4	400	3000	3000	None	18	0.935	7.696	0.42%	0.64%	428.2
Analysis 2											
	LPM	**Impeller (°)**	**Left RPM**	**Right RPM**	**Cage**	**LPA/RPA (mmHg)**	**Time (s): Mean**	**Time (s): Max**	**DI: Mean**	**DI: Max**	**Max Shear Stress**
7	3	200	3000	3000	None	18	0.805	2.834	0.24%	0.40%	541.8
8	3	300	3000	3000	None	18	0.791	2.849	0.20%	0.39%	511.8
9	3	500	3000	3000	None	18	0.890	3.896	0.23%	0.35%	260.9
Analysis 3											
	LPM	**Impeller (°)**	**Left RPM**	**Right RPM**	**Cage**	**LPA/RPA (mmHg)**	**Time (s): Mean**	**Time (s): Max**	**DI: Mean**	**DI: Max**	**Max Shear Stress**
10	3	400	3000	2000	None	18	1.062	7.666	0.14%	0.41%	281.0
11	3	400	3000	4000	None	18	0.840	2.414	0.30%	0.31%	453.5
Analysis 4											
	LPM	**Impeller (°)**	**Left RPM**	**Right RPM**	**Cage**	**LPA/RPA (mmHg)**	**Time (s): Mean**	**Time (s): Max**	**DI: Mean**	**DI: Max**	**Max Shear Stress**
12	3	400	3000	3000	Straight	18	0.719	2.104	0.19%	0.38%	257.9
13	3	400	3000	3000	Twisted	18	0.792	2.363	0.19%	0.29%	261.3
Analysis 5											
	LPM	**Impeller (°)**	**Left RPM**	**Right RPM**	**Cage**	**LPA/RPA (mmHg)**	**Time (s): Mean**	**Time (s): Max**	**DI: Mean**	**DI: Max**	**Max Shear Stress**
14	3	400	3000	3000	Straight	9	0.738	1.910	0.19%	0.41%	317.1
15	3	400	3000	3000	Straight	24	0.747	2.372	0.19%	0.38%	337.5

5. Discussion

5.1 Overview

Every year, there are 2000 single ventricle births. The treatment and management of patients with single ventricle physiology is expensive, with a cost of $1.4 billion yearly [3, 4]. Such severe cardiovascular defects often lead to a number of health complications, for which patients have to often undergo open-heart surgeries. These procedures culminate with a Fontan physiology, which although result in a functional cardiovascular system, comes with numerous long-term challenges. Fontan patients have long term symptoms such as abnormal cardiovascular hemodynamics, increased systemic venous pressure, supraventricular arrhythmias, reduced exercise capacity, and protein-losing enteropathy [2, 9]. Cardiac transplantation, often needed for Fontan patients, involve large wait times and require significant reconstruction of the veins and arteries, ultimately resulting in 44% operative mortality rates within Fontan patients [2, 9, 10].

This thesis discussed a novel stent and device combination design to address this problem. The device involves blood collection at the TCPC junction with a lumen stent, which is directed to and propelled by the axial blood flow pumps in the pulmonary arteries. This design hopes to augment energy in the system and generate the pressure needed to bring the physiology to near-normal conditions. The thesis involves a discussion of computational analyses through

the execution of 156 simulations to test pump performance while targeting design parameters.

5.2 Pressure and Energy Generations

In studying the effect of pump rotational speed and flow rate on pressure generation in Analysis 1 (**Figure 11** and **Figure 12**), increasing flow rate resulted in a decrease in pressure generation. This behavior is expected as based on the Navier-Stokes Equation. However this effect was diminished in the lowest rotational speed (2000 RPM). Additionally, pressure increased with greater rotational speeds. Based on the design criteria of 1 - 5mmHg pressure generation, 2000 RPM and 3000 RPM performed within the range for all flow rates, while 4000 RPM had significantly higher pressure generations. Similar results were found for Analysis 2: both 2000 and 3000 RPM performed in the range specified in the design criteria for all impeller degrees, while 4000 RPM showed significantly higher pressure increases than 1- 5mmHg (see **Figure 14**). In comparison, it can be seen in **Figure 19**, despite the decreases in pressure generation with the cage designs, all values met the design criteria of 1 - 5mmHg increase in pressure.

In comparing **Figure 16** and **Figure 17**, it can be seen that 1000 RPM differences between the two pump rotational speeds, when studying higher rotational speeds (3000 and 4000 RPM) resulted in a difference of approximately 3mmHg pressure difference in the left and right pump regions. However, when studying lower rotational speeds (2000 RPM and 3000 RPM) with a difference of

1000 RPM between the two pumps, a 2mmHg pressure difference was observed between the two regions. Rotational speed difference of 500 RPM resulted in a 1.5mmHg pressure difference in the left and right pump regions in both higher and lower rotational speeds (3500 and 3000 RPM vs 2500 and 3000 RPM). Thus, these results show that with lower rotational speeds, increasing differences between the pump rotational speeds do not have a significant impact on pressure differences in the two pump regions.

With high rotational speeds and low outlet pressures, pump rotation could result in a large pressure drop in the SVC and IVC. This can be a major concern as a severe pressure drop could result in the vessel to collapse. From **Figure 21**, it can be seen that with the lowest outlet pressure (9 mmHg) and highest rotational speed of 4000 RPM, SVC inlet pressure remains at 16.5 mmHg. Thus vessel suction is not a concern with this design and parameters.

In comparing cage designs, the straight cage showed higher pressure and energy rises than the twisted cage design. This is expected because the straight cage filaments redirect the blood flow by reducing its vorticity, thus supporting energy transfer. However, since the twisted cage filaments twist in the same direction of the blades, they do not redirect the blood flow, thus do not aid energy transfer.

As discussed in the results, significant increases in energy were observed both with increasing flow rates and increasing rotational speed (**Figure 13**). Similar to pressure augmentation, twist of pump blades had a positive relationship with energy increase until 300°. At higher degrees (400 and 500), an

inverse relationship existed between the blade twist and energy generation (**Figure 15**). This can be explained because a small number of blades provides lower amount of propulsion to the fluid. However, a large number of blades with minimal spacing in between restricts fluid flow within the passage, also resulting in a less effective pump. Thus, 300° seems to represent the optimal twist of blades. As seen in **Figure 20**, addition of a cage slightly reduced the impact of increasing flow rate on energy generation; however significant increases in energy did exist with increasing flow rate for both cage designs.

5.3 Blood Damage Analysis

As previously discussed, shear stresses below 425 Pa, exposure times below 620 ms, and blood damage indices below 2% were selected as design criterions for the blood pumps. As the results discussed, all mean exposure times exceeded the desired exposure time of 620 ms, since the lowest means were between 0.7 and 0.8 seconds. However, the commonality between the lowest exposure times were that they were all simulations including a straight cage or twisted cage support, further confirming the need for a cage support for the design. The twisted cage support had a slightly higher mean exposure time than the straight cage support, but a lower max damage index. This is expected because existing studies have also shown a twisted cage design with filaments twisting with the blades to perform poorly in comparison to other cage designs (including straight cage) [26]. Varying the impeller blade twist did not seem to show significant changes in exposure time (in comparing simulations #4, 7-9).

However increasing rotational speed of the pumps reduced the mean exposure time (in comparing simulations #3-5), as would be expected since the blood has more energy and is able to exit quicker. Examining the damage indices of all simulations showed that the max percentage was 0.64% (for simulation #6), which still remained below the 2% design criteria for the pumps. Many shear stress values were above the 425Pa criteria: Scenarios 5, 7, 8, and 11. Two of these scenarios had blade degree twists lower than 400 degrees, while the other two scenarios had one or two pumps rotating at 4000 RPM. This shows that lower degree twists and higher pump rotational speeds result in higher shear stresses.

6. Future Work and Conclusions

6.1 Limitations and Future Work

In this study, computational modeling was limited to examining pump performance in idealized and simplified conditions. As the boundary conditions, vessel walls were indicated as rigid bodies, and both the density and viscosity of blood were kept constant. Additionally, the analyses were done assuming steady state conditions. Further studies can examine transient flow conditions, vessel compliance conditions, and blood density and viscosity variability effects. Additionally, this study idealized the TCPC with complete alignment of the SVC and IVC. Future studies can alter the TCPC model to include a 1-diameter offset between the SVC and IVC central axes and/or consider an anatomical TCPC model. Pump performance can be further analyzed with this change, and rotational speeds of the left and right pumps can be varied according to the findings of Analysis 3 to accommodate this difference.

Additionally, hemolysis testing can be conducted per the ASTM standards discussed in Section 2.4. These experimental studies will allow further analysis of pump performance and comparisons with the numerical analyses executed in this thesis.

Multiple variations of cage design and degrees twist of the pump blades could not be analyzed due to time constraints. However, future studies can examine different configurations of the twisted cage design. This data showed

that the straight cage performed better than the twisted cage with filaments twisting in the same direction as the pump blades. However, the incorporation of a cage design resulted in a significant drop in pressure generation when compared to a no-cage design. Thus, a cage design that can enhance energy transfer while minimizing blood trauma is desired. Previous studies have examined numerous cage filament patterns that can also be analyzed for this design [26].

A study by Chopski et al. [33] examined degree twist of the blades for intravascular axial flow blood pump placement in the IVC. Interestingly, highest pressure generations were found with 380 and 400 degree twists. The findings of this thesis showed that 300 degrees twist had the highest pressure generation and 400 degrees twist performed lower than 200 degrees twist. This difference may be due to the novel stent and pump configuration, and also due to the difference in pump placement. Shear stresses may also need to be examined at smaller intervals as 300 and 400° twists had significantly different max shear stresses. Thus, future work can also further examine the effect of degree twist on pressure generation and shear stress by conducting simulations at 25° intervals between 200 and 400° to provide a more accurate estimation on the blade twist for the greatest pressure generation while maintaining low shear stresses.

6.2 Research Conclusions

Results found that increasing rotational speed resulted in significant increase in pressure, while increasing flow rate resulted in decrease in pressure. However, both parameters resulted in significant energy augmentations. Also, in comparison to 2000 and 4000 RPM, 3000 RPM showed lowest mean exposure time and shear stresses. Additionally, 300 degrees twist of the pump blades demonstrated highest pressure increases, but higher blade twists (400° and 500°) demonstrated lower shear stresses. Results also showed that pressure augmentations in the left and right pump regions showed the greatest difference when both pumps had high rotational speeds with a difference of 1000 RPM. Current cage study results supported existing cage design studies [26]. The results showed that the addition of a cage results in reduces blood damage and a cage with filaments twisting with the blades performs poorly in comparison to a straight filament cage. Although the addition of a cage reduced pressure augmentation, it also resulted in lower mean exposure times and shear stresses. Lastly, it was found that high pump rotational speeds did not result in negative pressures in the venae cavae. Based on the findings, the recommended design parameters for the axial pumps are 3000 RPM and 300-400° blade twist with a straight cage design. The results show successful initial performance of the novel device configuration, and suggestions are provided for further experimental testing and computational analysis. This thesis demonstrates significant potential of the design to address the current limitations in mechanical assist devices and provide bridge-to-transplant for Fontan patients.

List of References

[1] D. H. Kafagy, T. W. Dwyer, K. L. McKenna, J. P. Mulles, S. G. Chopski, W. B. Moskowitz*, et al.*, "Design of axial blood pumps for patients with dysfunctional Fontan physiology: computational studies and performance testing," *Artificial Organs,* vol. 39, pp. 34-42, January 2015.

[2] S. S. Bhavsar, J. Y. Kapadia, S. G. Chopski, and A. L. Throckmorton, "Intravascular mechanical cavopulmonary assistance for patients with failing Fontan physiology," *Artificial Organs,* vol. 33, pp. 977-987, November 2009.

[3] C. A. Russo and A. Elixhauser. (2007). Hospitalizations for birth defects, 2004. Healthcare Cost and Utilization Project [Online]. Available: http://www.hcup-us.ahrq.gov/reports/statbriefs/sb24.pdf [March 12, 2015].

[4] Columbus Ohio Adult Congenital Heart Disease Program (n.d.). Single ventricle defects [Online]. Available: https://www.nationwidechildrens.org/Document/Get/129477 [May 2016].

[5] Academic Dictionaries and Encyclopedias. (n.d.). Tricuspid valve [Online]. Available: http://en.academic.ru/dic.nsf/enwiki/149504 [March 12, 2015].

[6] M. Gewillig, "The Fontan circulation," *Heart (British Cardiac Society),* vol. 91, pp. 839-846, June 2005.

[7] The Children's Heart Clinic. (2012). Modified Fontan procedure (extracardiac conduit) [Online]. Available: http://www.childrensheartclinic.org/ProcedureIllustrations/Fontan.pdf [May 10, 2016].

[8] T. Takken, A. D. T. Harkel, N. Duppen, S. S. Bossers, I. M. Kuipers, M. Schokking*, et al.*, "Exercise capacity in children after total cavopulmonary connection: lateral tunnel versus extracardiac conduit technique," *Journal of Thoracic and Cardiovascular Surgery,* vol. 148, pp. 1490-1497, October 2014.

[9] A. L. Throckmorton, S. Lopez-Isaza, and W. Moskowitz, "Dual-pump support in the inferior and superior vena cavae of a patient-specific Fontan physiology," *Artificial Organs,* vol. 37, pp. 513-522, June 2013.

[10] M. Petko, R. J. Myung, G. Wernovsky, M. I. Cohen, J. Rychik, S. C. Nicolson*, et al.*, "Surgical reinterventions following the Fontan procedure," *European Journal of Cardio-Thoracic Surgery,* vol. 24, pp. 255-259, August 2003.

[11] K. L. Rood, S. A. Teele, C. S. Barrett, J. W. Salvin, P. T. Rycus, F. Fynn-Thompson*, et al.*, "Extracorporeal membrane oxygenation support after the Fontan operation," *The Journal of Thoracic and Cardiovascular Surgery,* vol. 142, pp. 504-510, September 2011.

[12] S. D. Gregory, D. Timms, N. Gaddum, D. G. Mason, and J. F. Fraser, "Biventricular assist devices: a technical review," *Annals of Biomedical Engineering,* vol. 39, pp. 2313-2328, September 2011.

[13] B. Stiller, I. Adachi, and C. D. Fraser, "Pediatric ventricular assist devices," *Pediatric Critical Care Medicine,* vol. 14, pp. S20-S26, June 2013.

[14] S. Weinstein, R. Bello, C. Pizarro, F. Fynn-Thompson, J. Kirklin, K. Guleserian*, et al.*, "The use of the Berlin Heart EXCOR in patients with functional single ventricle," *Journal of Thoracic and Cardiovascular Surgery,* vol. 147, pp. 697-704, February 2014.

[15] A. L. Throckmorton and S. G. Chopski, "Pediatric circulatory support: current strategies and future directions. Biventricular and univentricular mechanical assistance," *ASAIO Journal,* vol. 54, pp. 491-497, September 2008.

[16] F. G. Lacour-Gayet, C. J. Lanning, S. Stoica, R. Wang, B. A. Rech, S. Goldberg*, et al.*, "An artificial right ventricle for failing Fontan: in vitro and computational study," *The Annals of Thoracic Surgery,* vol. 88, pp. 170-176, July 2009.

[17] R. B. Medvitz, D. A. Boger, V. Izraelev, G. Rosenberg, and E. G. Paterson, "Computational fluid dynamics design and analysis of a passively suspended Tesla pump left ventricular assist device," *Artificial Organs,* vol. 35, pp. 522-533, May 2011.

[18] D. Wang, M. Plunkett, J. Lynch, X. Zhou, C. Ballard-Croft, and J. B. Zwischenberger, "Wang-Zwische double-lumen cannula leads to total cavopulmonary support in a failing Fontan sheep model," *The Annals of Thoracic Surgery,* vol. 91, pp. 1956-1960, June 2011.

[19] D. Wang, G. Gao, M. Plunkett, G. Zhao, S. Topaz, C. Ballard-Croft*, et al.*, "A paired membrane umbrella double-lumen cannula ensures consistent cavopulmonary assistance in a Fontan sheep model," *The Journal of Thoracic and Cardiovascular Surgery,* vol. 148, pp. 1041-1047, September 2014.

[20] G. A. Giridharan, S. C. Koenig, J. Kennington, M. A. Sobieski, J. Chen, S. H. Frankel*, et al.*, "Performance evaluation of a pediatric viscous impeller pump for Fontan cavopulmonary assist," *The Journal of Thoracic and Cardiovascular Surgery,* vol. 145, pp. 249-257, January 2013.

[21] R. Wang, F. G. Lacour-Gayet, C. J. Lanning, B. A. Rech, P. J. Kilfoil, J. Hertzberg*, et al.*, "Initial experience with the development and numerical and in vitro studies of a novel low-pressure artificial right ventricle for pediatric Fontan patients," *ASAIO Journal,* vol. 52, pp. 682-692, November 2006.

[22] M. D. Rodefeld, J. H. Boyd, C. D. Myers, B. J. LaLone, A. J. Bezruczko, A. W. Potter*, et al.*, "Cavopulmonary assist: circulatory support for the univentricular fontan circulation," *The Annals of Thoracic Surgery,* vol. 76, pp. 1911-1916, December 2003.

[23] A. L. Throckmorton, J. Y. Kapadia, S. G. Chopski, S. S. Bhavsar, W. B. Moskowitz, S. D. Gullquist*, et al.*, "Numerical, hydraulic, and hemolytic evaluation of an intravascular axial flow blood pump to mechanically support Fontan patients," *Annals of Biomedical Engineering,* vol. 39, pp. 324-336, January 2011.

[24] A. L. Throckmorton, S. Lopez-Isaza, E. A. Downs, S. G. Chopski, J. J. Gangemi, and W. Moskowitz, "A viable therapeutic option: mechanical circulatory support of the failing Fontan physiology," *Pediatric Cardiology,* vol. 34, pp. 1357-1365, August 2013.

[25] S. G. Chopski, O. M. Rangus, E. A. Downs, W. B. Moskowitz, and A. L. Throckmorton, "Three-dimensional laser flow measurements of a patient-specific Fontan physiology with mechanical circulatory assistance," *Artificial Organs,* vol. 39, pp. E67-E78, June 2015.

[26] A. L. Throckmorton, E. A. Downs, J. A. Hazelwood, J. O. Monroe, and S. G. Chopski, "Twisted cardiovascular cages for intravascular axial flow blood pumps to support the Fontan physiology," *Artificial Organs,* vol. 35, pp. 369-375, May 2012.

[27] A. L. Throckmorton, J. P. Carr, W. B. Moskowitz, J. J. Gangemi, C. M. Haggerty, and A. P. Yoganathan, "Uniquely shaped cardiovascular stents enhance the pressure generation of intravascular blood pumps," *The Journal of Thoracic and Cardiovascular Surgery,* vol. 144, pp. 704-709, September 2012.

[28] A. L. Throckmorton, J. P. Carr, S. A. Tahir, R. Tate, E. A. Downs, S. S. Bhavsar*, et al.*, "Mechanical cavopulmonary assistance of a patient-specific Fontan physiology: numerical simulations, lumped parameter modeling, and suction experiments," *Artificial Organs,* vol. 35, pp. 1036-1047, November 2011.

[29] R. Paul, J. Apel, S. Klaus, F. Schugner, P. Schwindke, and H. Reul, "Shear stress related blood damage in laminar couette flow," *Artificial Organs,* vol. 27, pp. 517-529, June 2003.

[30] X. Song, A. L. Throckmorton, H. G. Wood, J. F. Antaki, and D. B. Olsen, "Computational fluid dynamics prediction of blood damage in a centrifugal pump," *Artificial Organs,* vol. 27, pp. 938-941, October 2003.

[31] V. E. Hjortdal, K. Emmertsen, E. Stenbøg, T. Fründ, M. R. Schmidt, O. Kromann*, et al.*, "Effects of exercise and respiration on blood flow in total cavopulmonary connection: a real-time magnetic resonance flow study," *Circulation,* vol. 108, pp. 1227-1231, September 2003.

[32] S. S. Bhavsar, W. B. Moskowitz, and A. L. Throckmorton, "Interaction of an idealized cavopulmonary circulation with mechanical circulatory assist using an intravascular rotary blood pump," *Artificial Organs,* vol. 34, pp. 816-827, October 2010.

[33] S. G. Chopski, C. S. Fox, M. L. Riddle, K. L. McKenna, J. P. Patel, J. T. Rozolis*, et al.*, "Pressure–flow experimental performance of new intravascular blood pump designs for Fontan patients," *Artificial Organs,* vol. 40, pp. 233-242, March 2016.

[34] R. E. Klabunde. (n.d.). *Pulmonary Arterial Pressure* [Online]. Available: http://www.cvpharmacology.com/clinical%20topics/pulmonary%20hypertension [2016].

[35] LiDCO Group plc. (n.d.). Normal hemodynamic parameters [Online]. Available: http://www.lidco.com/clinical/hemodynamic.php [April 23, 2016].

[36] M. Beghetti, "Fontan and the pulmonary circulation: a potential role for new pulmonary hypertension therapies," *Heart (British Cardiac Society),* vol. 96, pp. 911-916, June 2010.

[37] T. C. Slesnick and A. P. Yoganathan, "Computational modeling of Fontan physiology: at the crossroads of pediatric cardiology and biomedical engineering," *The International Journal of Cardiovascular Imaging,* vol. 30, pp. 1073-1084, August 2014.

[38] A. L. Throckmorton, "Computational design and experimental hydraulic testing of an axial flow ventricular assist device for infants and children," PhD Dissertation, University of Virginia, 2006.

[39] O. Zikanov, *Essential computational fluid dynamics* vol. 1. Hoboken, N.J: Wiley, 2010.

[40] A. L. Throckmorton and A. Untaroiu, "CFD analysis of a Mag-Lev ventricular assist device for infants and children: fourth generation design," *ASAIO Journal,* vol. 54, pp. 423-431, 2008.

[41] S. S. Varghese and S. H. Frankel, "Numerical modeling of pulsatile turbulent flow in stenotic vessels," *Journal of Biomechanical Engineering,* vol. 125, pp. 445-460, August 2003.

[42] X. Song, A. L. Throckmorton, H. G. Wood, J. F. Antaki, and D. B. Olsen, "Quantitative evaluation of blood damage in a centrifugal VAD by computational fluid dynamics," *Journal of Fluids Engineering,* vol. 126, pp. 410-418, July 2004.

[43] G. Heuser and R. Opitz, "A Couette viscometer for short time shearing of blood," *Biorheology,* vol. 17, pp. 17-24, 1980.